

# Antioxidant Microgels Support Peroxide-Challenged Hepatic Cells

Isabella Nymann Westensee, Karen Louise Thomsen, Rajeshwar Prosad Mookerjee, and Brigitte Städler\*

Access to therapeutic strategies that counter cellular stress induced by reactive oxygen species (ROS) is an important, long-standing challenge. Here, the assembly of antioxidant artificial cells is based on alginate hydrogels equipped with non-native catalysts, namely platinum nanoparticles and an EUK compound. These artificial cells are able to preserve the viability and lower the intracellular ROS levels of challenged hepatic cells by removing peroxides from the extracellular environment. Conceptually, this strategy illustrates the potential use of artificial cells with a synthetic catalyst toward long-term support of hepatic cells and potentially other mammalian cells.

## 1. Introduction

Oxidative stress and inflammation play an important role in the advancement of liver diseases. The nanocarrier mediated intracellular delivery of antioxidants to the liver was recently reviewed by Li et al.<sup>[1]</sup> and Liu et al.<sup>[2]</sup> Current treatment guidance uses N-acetyl cysteine for the management of acetaminophen induced acute liver failure, which targets the depletion of glutathione for cell metabolism, but does nothing to counter the ongoing reactive oxygen species (ROS) production through cellular damage. Consequently, extracellular scavenging of ROS is envisioned to rejuvenate the liver milieu. However, past and current strategies of extracorporeal liver support devices have not specifically designed antioxidant capabilities but have relied on the capacity of

albumin dialysis to remove toxins and promote antioxidative and immunomodulatory effects. Despite this, no unequivocal clear evidence has been shown for improved survival for such patients with extracorporeal support.<sup>[3]</sup>

From a different perspective, artificial cells (ACs) are micron-sized assemblies that are envisioned to replace, enhance, or even add non-native activity upon interfacing with their living counterparts. Over the past years, many types of ACs were developed with increasing complexity aiming for the mimicry of cellular


function as recently discussed in several comprehensive reviews.<sup>[4–8]</sup> However, the direct interaction of ACs with mammalian cells has only started to be explored.<sup>[9]</sup> For example, ACs capable of communicating and exchanging chemical information with mammalian cells have recently been demonstrated with alginate-based ACs capable of eavesdropping on the hepatic activity of HepG2 cells, by releasing sender molecules that react with a conversion product from the hepatocytes, and in turn convert the product to luminescence.<sup>[10]</sup> Further, giant unilamellar vesicle (GUV)-based ACs producing H<sub>2</sub>O<sub>2</sub> by encapsulated catalysis were demonstrated, with H<sub>2</sub>O<sub>2</sub> utilized by red blood cells as peroxidase agents to convert Amplex Red to resorufin,<sup>[11]</sup> and brain-derived neurotrophic factor producing ACs to drive differentiation of neural stem cells.<sup>[12]</sup> Additionally, ACs capable of providing a supportive, therapeutic function to mammalian cell counterparts include the use of alginate-based ACs loaded with matrix vesicles (purified from cell culture) co-cultured with osteoblasts for enhanced biomineralization;<sup>[13]</sup> combating excitotoxicity in neuroblastoma cells with polystyrene-based ACs loaded with platinum nanoparticles that remove exogenous hydrogen peroxide (H<sub>2</sub>O<sub>2</sub>) and ammonia;<sup>[14,15]</sup> microsphere-based artificial stem cells that release Tβ4-exosomes to improve the angiogenic capacity of coronary endothelial cells;<sup>[16]</sup> prototissue of nitric oxide (NO) producing GUVs capable of relaxing rat blood vessels *ex vivo*;<sup>[17]</sup> ACs producing insulin precursor/insulin under hyperglycemic conditions to promote glucose uptake in MCF-7 cells;<sup>[18]</sup> erythrocyte membrane fragment coated coacervates producing NO for blood vessel vasodilation in rabbits,<sup>[19]</sup> and proangiogenic GUV-based ACs expressing a fibroblast growth factor which when suspended in matrigel and injected into mice, enables blood venule infiltration.<sup>[20]</sup>

Specifically relevant in the context here are our prior efforts where HepG2 cells were co-cultured with catalytically active ACs, e.g., alginate-based ACs functionalized with metalloporphyrins

I. N. Westensee, B. Städler  
Interdisciplinary Nanoscience Center (iNANO)  
Aarhus University  
Gustav Wieds Vej 14, Aarhus 8000, Denmark  
E-mail: [bstadler@inano.au.dk](mailto:bstadler@inano.au.dk)

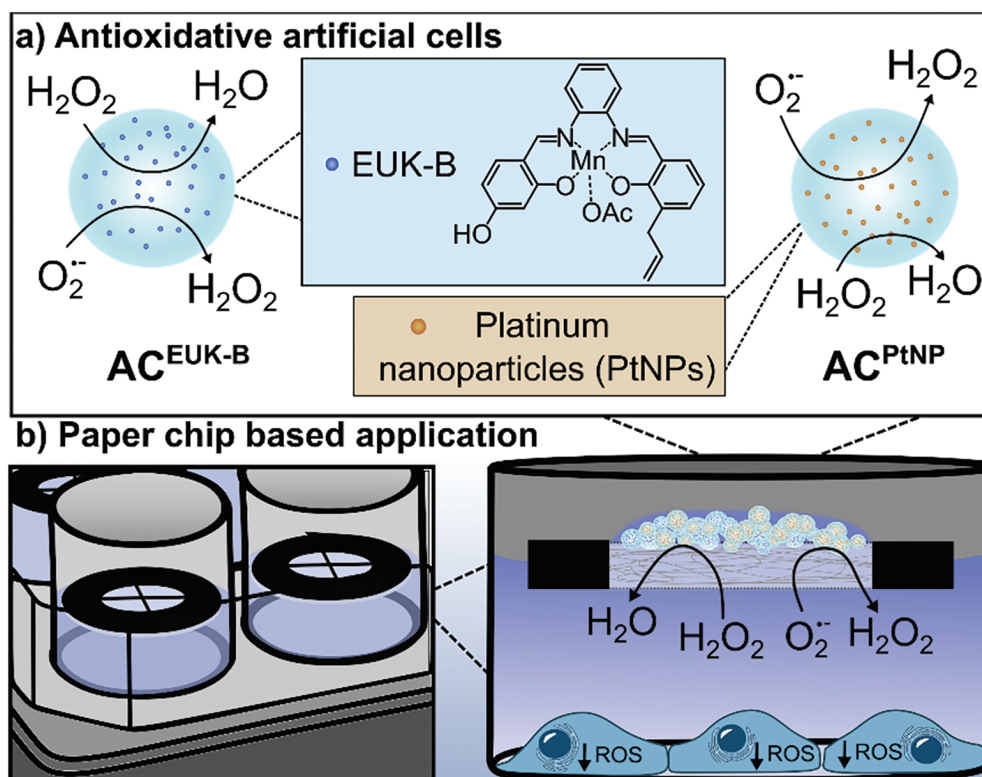
K. L. Thomsen  
Department of Hepatology and Gastroenterology  
Aarhus University Hospital  
Palle Juul-Jensens Boulevard 99, Aarhus N 8200, Denmark

R. P. Mookerjee  
Institute for Liver and Digestive Health  
University College London  
Royal Free Campus, Rowland Hill Street, Hampstead, London NW3 2PF, UK

 The ORCID identification number(s) for the author(s) of this article can be found under <https://doi.org/10.1002/adbi.202300547>

© 2024 The Authors. Advanced Biology published by Wiley-VCH GmbH. This is an open access article under the terms of the [Creative Commons Attribution](https://creativecommons.org/licenses/by/4.0/) License, which permits use, distribution and reproduction in any medium, provided the original work is properly cited.

DOI: 10.1002/adbi.202300547



**Scheme 1.** a) The manganese–salen compound EUK-B and PtNPs are encapsulated in microgel-based ACs termed AC<sup>EUK-B</sup> and AC<sup>PtNP</sup>, respectively, which convert O<sub>2</sub><sup>-</sup> to H<sub>2</sub>O<sub>2</sub>, and H<sub>2</sub>O<sub>2</sub> to H<sub>2</sub>O and oxygen. b) The ACs are applied to floating paper chips at the liquid–air interface of the cell media in wells with cultured hepatocytes stressed with H<sub>2</sub>O<sub>2</sub> or tert-butyl hydroperoxide (tBuOOH).

transferring a fluorescent signal to HepG2 cells,<sup>[21]</sup> and ACs with encapsulated catalase co-cultured in cell aggregates with HepG2 cells to alleviate oxidative stress, through the dismutation of H<sub>2</sub>O<sub>2</sub> to H<sub>2</sub>O and O<sub>2</sub> by catalase.<sup>[22,23]</sup> However, in the latter case, the short life-time of catalase limited the benefits of the ACs substantially. This limitation can be overcome by the use of artificial enzymes, which mimic the catalytic activity of natural antioxidative enzymes but exhibit greater stability and maintained function over time.<sup>[8]</sup> Thus, ACs functionalized with antioxidative artificial enzymes have the potential to offer a complementary approach for the design of extracorporeal liver support devices with long-lasting functionality, compared to exhaustible albumin-based dialysis systems.

In this study, the aim was to assemble and characterize antioxidant alginate microgel-based ACs using a manganese–salen compound EUK-B, or platinum nanoparticles (PtNPs), as artificial antioxidant enzymes to alleviate the extracellular oxidative stress on hepatic cells. Floating paper chips were used as a facile method for the immobilization of ACs, and for placing them in close proximity with the extracellular space of cultured hepatocytes. Specifically, we: i) evaluated the ability of EUK-B and PtNP-loaded ACs to convert superoxide anions (O<sub>2</sub><sup>-</sup>) to H<sub>2</sub>O<sub>2</sub>, and H<sub>2</sub>O<sub>2</sub> to water extracellularly (Scheme 1a); and ii) explored whether antioxidant ACs can be loaded onto floating paper chips and rescue peroxide challenged HepG2 cell and HHL-5 cells cultured in proximity, by not only improving their viability but also lowering the intracellular oxidative stress (Scheme 1b).

## 2. Results and Discussion

### 2.1. Assembly of Antioxidant Microgels

Two different moieties, namely PtNP and an EUK derivative, were chosen due to their known SOD-like and catalase-like activity, and were compared for their ability to provide the active part in the antioxidant microgels. PtNPs exhibit peroxidase-like activity (producing ·OH) under acidic conditions and catalase-like activity (producing H<sub>2</sub>O and O<sub>2</sub>) as well as SOD-like activity (scavenging O<sub>2</sub><sup>-</sup>) at neutral and alkaline conditions.<sup>[24]</sup> Several examples illustrated that intracellularly placed PtNPs reduced oxidative stress-mediated cell damage and cell death.<sup>[25–28]</sup> Additionally, PtNPs immobilized on polystyrene carriers were also employed to extracellularly lower ROS levels with the aim to mitigate excitotoxicity in neuroblastoma cells,<sup>[14]</sup> and later in rat primary cortical neurons.<sup>[15]</sup> Here, PtNPs were fabricated according to a previously published protocol,<sup>[14]</sup> and imaged by transmission electron microscopy, revealing a size of ≈4 nm (Figure S1, Supporting Information).

Alternatively, manganese–salen complexes are small antioxidant compounds, first reported in the 1930s<sup>[29]</sup> and are currently experiencing a renaissance.<sup>[30]</sup> Examples of the beneficial effect of EUK-134 from the past 10 years include the lowering of the level of lipid peroxides at the surface of UVA-exposed skin,<sup>[31]</sup> the treatment of zinc and paraquat induced oxidative stress in polymorphonuclear leukocytes,<sup>[32]</sup> the attenuation of

lipopolysaccharide-induced increase in pulmonary artery pressure in a porcine model of sepsis,<sup>[33]</sup> and suppressive effects of ionizing radiation on mitochondrial function in rat astrocyte cultures.<sup>[34]</sup> Further, EUK-134 were loaded into PEG liposomes for endothelial targeting,<sup>[35]</sup> or conjugated to lipophilic cations aiming at improving mitochondrial delivery.<sup>[36]</sup> A particularly interesting example was reported by Rezazadeh et al. who found that EUK-8 and EUK-134 improved steatosis, ballooning and inflammation in the liver of rats with NASH.<sup>[37]</sup> We recently synthesized a variety of modified EUK compounds with enhanced electron-donor abilities compared to EUK-134, and with pendant groups that improve their water solubility.<sup>[38]</sup> Among them, EUK-B showed the best balance between the catalytic activity and the water solubility and was therefore, chosen here.

First, the H<sub>2</sub>O<sub>2</sub> conversion activity of 0.1 mg mL<sup>-1</sup> PtNPs or EUK-B in PBS was compared (Figure S2a, Supporting Information). It was found that PtNPs in solution were more efficient for a given mass concentration, i.e., PtNPs converted 82 μM H<sub>2</sub>O<sub>2</sub> min<sup>-1</sup>, while EUK-B removed 54 μM H<sub>2</sub>O<sub>2</sub> min<sup>-1</sup> from a 1 mM H<sub>2</sub>O<sub>2</sub> solution.

For the next step in experimentation, the PtNPs and EUK-B were encapsulated in alginate particles to form antioxidative microgels. Alginate is an FDA approved polysaccharide used for a variety of applications as outlined by Lee and Mooney,<sup>[39]</sup> and has previously been used by us to successfully fabricate ACs appropriate for interfacing with biological cells.<sup>[10,13,21,22]</sup> The PtNPs or EUK-B were dispersed in an alginate solution made from a mixture of low and high molecular weight alginate, with high α-L-guluronate content. Specifically, alginate was directly dissolved in the stock solution of PtNPs, which corresponded to a PtNP concentration of ≈1 mg mL<sup>-1</sup>, while dissolved alginate was added to a solution of EUK-B, resulting in an EUK-B concentration of ≈0.5 mg mL<sup>-1</sup>. These solutions were used to make alginate-based microgels with an extrusion-dripping method using an Encapsulator B-390. The alginate solution was extruded through a nozzle, forming droplets due to an applied vibrational frequency, which were crosslinked in a calcium bath to yield AC<sup>PtNP</sup> and AC<sup>EUK-B</sup>. The encapsulation efficiency was evaluated via visual inspection by comparing the colour originating from non-encapsulated PtNPs or EUK-B in the supernatant after 0, 5, or 365 days (Figure S3a, Supporting Information). The supernatant consisted of the crosslinking bath on day 0, and the storage buffer at day 5 and 365. No non-encapsulated PtNP could be observed in the supernatants of AC<sup>PtNP</sup> even after 365 days, while AC<sup>EUK-B</sup> showed trace amounts of non-encapsulated EUK-B in the crosslinking bath, and negligible amounts were observed to have leaked after 365 days.

Additionally, non-loaded alginate microgels made of only alginate were made as controls and referred to as AC<sup>0</sup>. The PtNPs were distributed evenly throughout the microgels without visible aggregation, while the EUK-B appeared in aggregates within the hydrogel network (Figure S3b, Supporting Information). AC<sup>0</sup> and AC<sup>PtNP</sup> showed two populations in their size distribution (AC<sup>0</sup> diameters of ≈100 μm and 150 μm; AC<sup>PtNP</sup> diameters of ≈130 and 230 μm). In contrast, AC<sup>EUK-B</sup> was a single population with diameters of ≈80 μm (Figure S3c, Supporting Information). This observation was likely due to the fact that dissolving EUK-B in alginate prior to microgel formation yielded a noticeably less viscous solution compared to pristine alginate solution (or

a PtNP-containing alginate solution), resulting in different types of microgels.

Next, the capability of AC<sup>EUK-B</sup> and AC<sup>PtNP</sup> to remove H<sub>2</sub>O<sub>2</sub> was evaluated. H<sub>2</sub>O<sub>2</sub> is a physiologically relevant, long-lived ROS produced by several enzymes/processes in the cells, including NADPH oxidases, the electron transport chain in mitochondria, the endoplasmic reticulum (ER) oxidoreductin, and cytochrome P450 enzymes in the ER. H<sub>2</sub>O<sub>2</sub> can diffuse through cells and tissues to mediate intercellular effects.<sup>[40]</sup> However, excess H<sub>2</sub>O<sub>2</sub> can initiate a cascade of reactions involving partially reduced transition metal ions, such as Fe<sup>2+</sup> or Cu<sup>+</sup>, leading to the generation of reactive hydroxyl radicals (-OH).<sup>[41]</sup> The presence of these radicals promotes the propagation of oxidative stress both intracellularly and extracellularly, attributed to H<sub>2</sub>O<sub>2</sub> membrane permeability. Consequently, H<sub>2</sub>O<sub>2</sub> is an important extracellular ROS target for the microgels. The H<sub>2</sub>O<sub>2</sub> removal ability of the microgels was determined by loading 100 mg AC microgels on floating paper chips placed in the wells of a 12-well plate containing either 1.5 mL PBS buffer (Figure 1ai) or cell media (Figure 1aiii) spiked with 1 mM H<sub>2</sub>O<sub>2</sub>. The floating paper chips were made by printing a ring onto paper in a regular ink jet printer followed by autoclaving to melt the ink particles into a hydrophobic barrier.<sup>[42]</sup> The H<sub>2</sub>O<sub>2</sub> consumption of AC<sup>EUK-B</sup> and AC<sup>PtNP</sup> after 1, 3, 6 and 8 h was comparable in PBS and cell media, i.e., the possible protein corona formation on PtNPs in cell media did not affect the performance of the surface catalyst. As expected, AC<sup>0</sup> did not lower the H<sub>2</sub>O<sub>2</sub> concentration. However, there is a trend for more efficient H<sub>2</sub>O<sub>2</sub> removal by AC<sup>EUK-B</sup> than AC<sup>PtNP</sup>, an effect that was statistically significant in both PBS and cell media. The initial removal of H<sub>2</sub>O<sub>2</sub> in cell media by AC<sup>EUK-B</sup> and AC<sup>PtNP</sup> was ≈0.23 and ≈0.12 mM H<sub>2</sub>O<sub>2</sub> per hour, respectively, which was determined by fitting the slope of the curve from 0 to 3 h with linear regression. The difference in activity was likely explained by the alginate affecting the surface catalysis of AC<sup>PtNP</sup>. This was supported by the observation that PtNP exhibited greater activity than an equivalent mass concentration of EUK-B in solution (Figure S2, Supporting Information). Additionally, AC<sup>PtNP</sup> encapsulated approximately twice the mass of catalyst compared to AC<sup>EUK-B</sup> (≈1 mg mL<sup>-1</sup> and 0.5 mg mL<sup>-1</sup>, respectively). The marginal EUK-B leakage observed for AC<sup>EUK-B</sup> in comparison to AC<sup>PtNP</sup> was considered negligible (Figure S3a, Supporting Information). It should also be noted that the comparison of mass loading efficiency between the surface and small molecule-based catalyst was chosen due to the observed aggregation of EUK-B in the AC<sup>EUK-B</sup>, which challenged a direct comparison of available catalytic sites in the two microgels. Further, the smaller size of AC<sup>EUK-B</sup> compared to AC<sup>PtNP</sup> might also have contributed to the increased activity in the former case due to the more free diffusion of H<sub>2</sub>O<sub>2</sub> in the microgels. Taken together, AC<sup>EUK-B</sup> exhibited higher catalytic activity.

In addition, the SOD-like activity of AC<sup>EUK-B</sup> and AC<sup>PtNP</sup> was evaluated in the same set-up in PBS using 10–100 mg microgels per paper chip (Figure 1b), corresponding to ≈0.01 mg–0.1 mg or 0.005 mg–0.05 mg PtNP or EUK-B, respectively. We would like to note that the SOD-like activity could not be evaluated in cell media because the xanthine oxidase enzyme that produce O<sub>2</sub><sup>-</sup> was not active. AC<sup>0</sup> exhibited no O<sub>2</sub><sup>-</sup> scavenging ability, while already 10 mg AC<sup>EUK-B</sup> and AC<sup>PtNP</sup> reached ≈70% SOD-like activity that increased to 95% for 100 mg AC. Initially, AC<sup>EUK-B</sup> resulted in

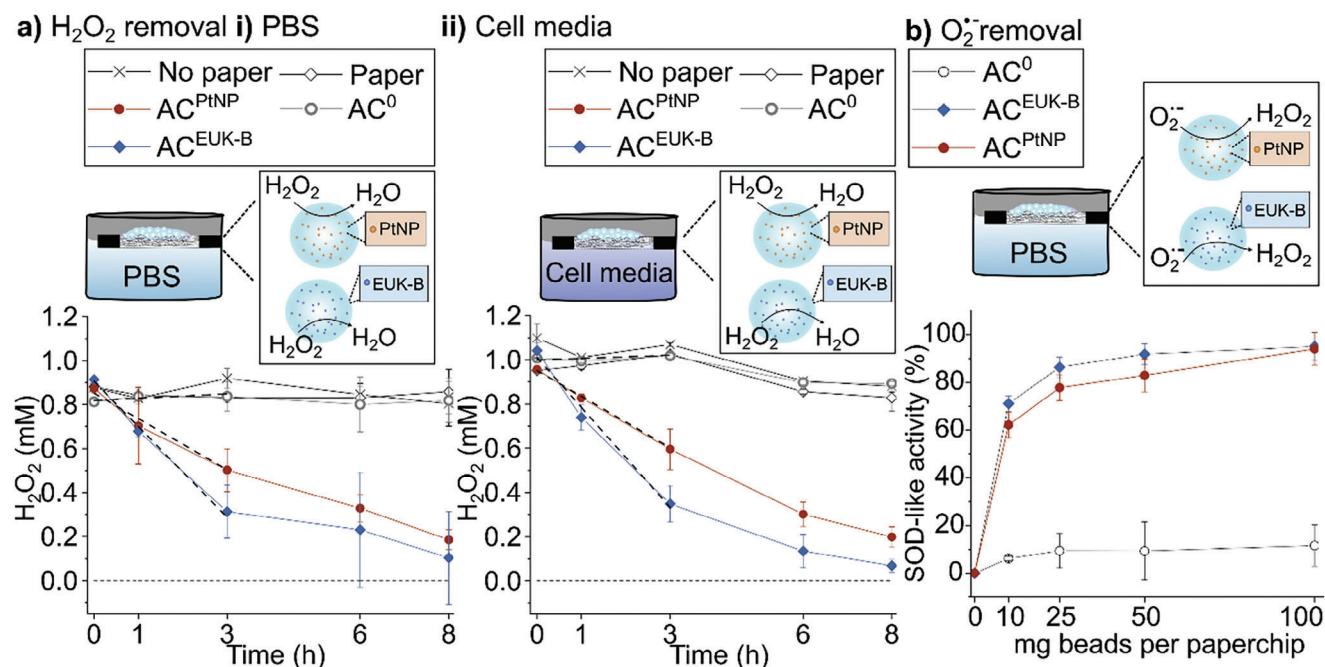


**Figure 1.** ROS removal of antioxidative microgels. a) H<sub>2</sub>O<sub>2</sub> removal of AC<sup>0</sup>, AC<sup>PtNP</sup>, and AC<sup>EUK-B</sup> over 8 h in PBS (i) or cell media (ii). The initial slope of the curve (from 0 h to 3 h) was fitted using linear regression. (*n* = 3). b) O<sub>2</sub><sup>•-</sup> removal is given as SOD-like activity (%) after 30 min of different amounts of microgels on paper chips (*n* = 3).

≈10% higher SOD activities compared to AC<sup>PtNP</sup>, probably due to the alginate network affected the surface catalytic activity of the PtNPs as outlined for the catalase-like activity.

## 2.2. Effect of Antioxidant Microgels on H<sub>2</sub>O<sub>2</sub>-Challenged HepG2 Cells

Following on, the aim was to rescue H<sub>2</sub>O<sub>2</sub>-challenged HepG2 cells using the floating paper chips loaded with AC<sup>PtNP</sup> and AC<sup>EUK-B</sup> (Figure 2a). Specifically, HepG2 cells were exposed to three doses of either 0.2 or 0.3 mM H<sub>2</sub>O<sub>2</sub> in 3 h intervals, in the presence of floating paper chips loaded with either 100 mg AC<sup>0</sup>, AC<sup>EUK-B</sup>, AC<sup>PtNP</sup> or a mixture of 50 mg AC<sup>EUK-B</sup>, and 50 mg AC<sup>PtNP</sup> (referred to as AC<sup>EUK-B/PtNP</sup>), before the HepG2 cell viability was assessed (Figure 2b). Several doses of H<sub>2</sub>O<sub>2</sub> were used to ensure continuous exposure of the cells to H<sub>2</sub>O<sub>2</sub>, which is known to spontaneously decompose in cell media. As expected, the empty and AC<sup>0</sup>-loaded paper chip had comparable reduction in HepG2 cell viability upon exposure to H<sub>2</sub>O<sub>2</sub> concentrations. There was not a significant difference in HepG2 cell viability depending on the type of microgel-loaded paper chips when 0.2 mM was used as the challenger (Figure 2bi). In contrast, there was a significant increase in HepG2 cell viability of ≈ 40% in the presence of AC<sup>EUK-B</sup> or AC<sup>EUK-B/PtNP</sup> when the cells were exposed to 0.3 mM H<sub>2</sub>O<sub>2</sub> (Figure 2bii). However, AC<sup>PtNP</sup> did not lead to a significant increase in viability, confirming the higher activity of AC<sup>EUK-B</sup>. Furthermore, this result also suggested that 50 mg AC<sup>EUK-B</sup> was already enough to remove the added amount of H<sub>2</sub>O<sub>2</sub>. With the aim of confirming this observation, the viability of HepG2 cells that were challenged with H<sub>2</sub>O<sub>2</sub> in the presence of paper chips

that were loaded with 50 mg AC<sup>EUK-B</sup> and 50 mg AC<sup>0</sup> (referred to as AC<sup>EUK-B/0</sup>) were determined. AC<sup>EUK-B/0</sup> resulted in a ≈30% increase in HepG2 cell viability compared to the control. This improved viability was not statistically significantly different from AC<sup>EUK-B</sup> or AC<sup>EUK-B/PtNP</sup>, suggesting that AC<sup>EUK-B</sup> were the major contributor to the HepG2 cell rescue. Consequently, only AC<sup>EUK-B</sup> was considered for the subsequent experiments.

Next, the benefit of AC<sup>EUK-B</sup> on the HepG2 cell viability was evaluated when exposed to H<sub>2</sub>O<sub>2</sub> over longer time. Specifically, HepG2 cells were exposed to three doses of H<sub>2</sub>O<sub>2</sub> between 0.1 and 0.5 mM every 3 h in the presence of the AC<sup>EUK-B</sup>-loaded paper chips, before the HepG2 cells were allowed to recover for 48 h in fresh media. Subsequently, the HepG2 cells were exposed to an additional two doses of H<sub>2</sub>O<sub>2</sub> over 6 h, either with the AC<sup>EUK-B</sup>-loaded paper chips present or after they were removed, before the HepG2 cell viability was determined (Figure 2ci). The resulting dose response curves revealed that HepG2 cells had the highest viability when the AC<sup>EUK-B</sup>-loaded paper chips were present the entire duration of the experiment with a half maximal effective concentration EC<sub>50</sub> of ≈226 μM (Figure 2cii). The EC<sub>50</sub> exhibited a statistically significant reduction to ≈177 μM when the AC<sup>EUK-B</sup>-loaded paper chips were removed following the 48 h recovery period. Conversely, when HepG2 cells were exposed to the treatment without paper chips, their EC<sub>50</sub> was notably lower at ≈128 μM. We have previously shown that catalase-loaded alginate microreactors in direct co-culture with HepG2 cells improved their cell viability when challenged with H<sub>2</sub>O<sub>2</sub> for 24 h. This supportive effect was not present anymore after 48 h co-culture, likely due to the activity loss of catalase.<sup>[22]</sup> Here, the AC<sup>EUK-B</sup> was found to be active even after 4 days in culture, demonstrating the benefit of longer lasting artificial enzymes.

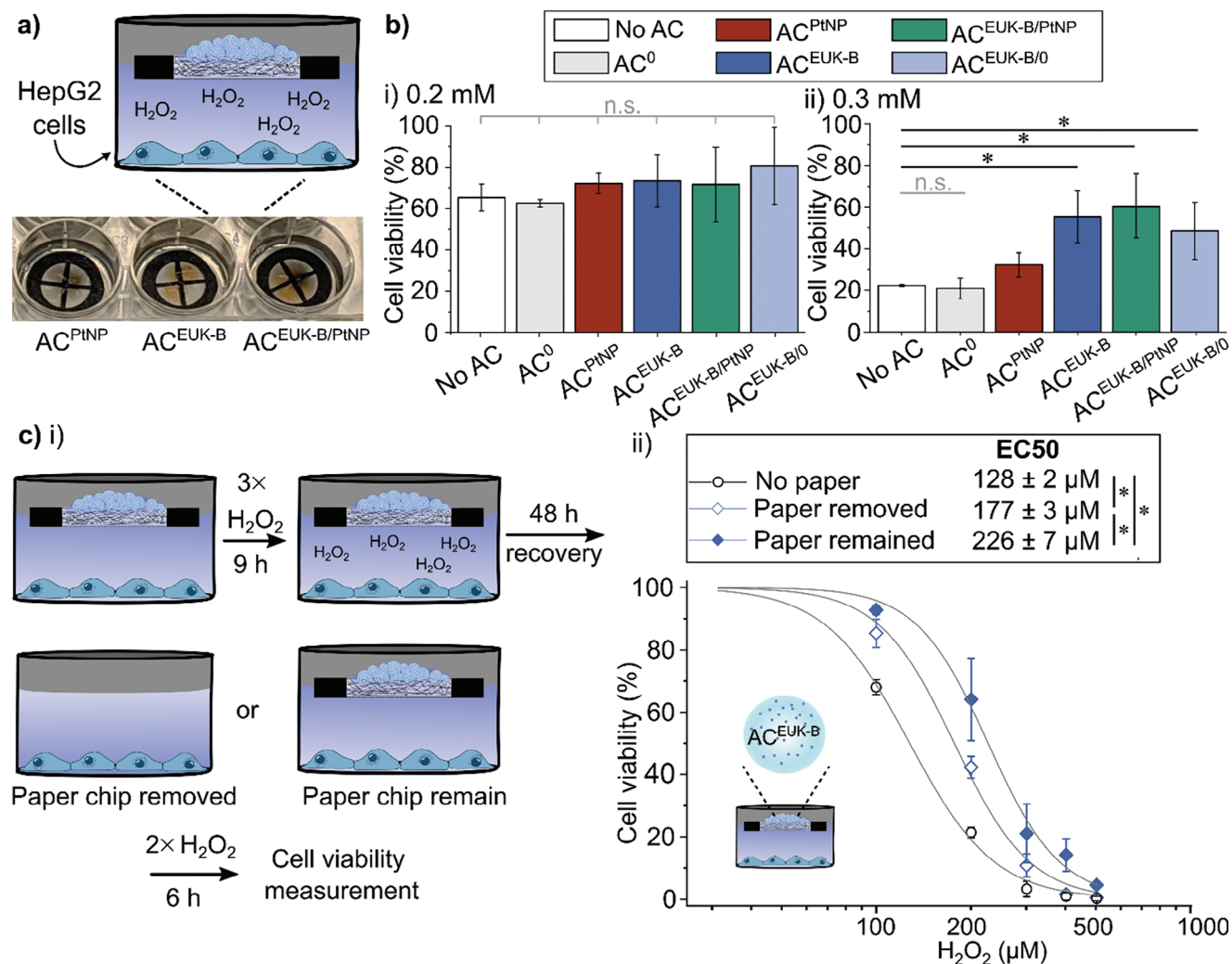


**Figure 2.** a) HepG2 cells were cultured in 12-well plates, and a floating paper chip was added to each well loaded with AC<sup>0</sup>, AC<sup>EUK-B</sup>, AC<sup>PtNP</sup> or a mixture of AC<sup>EUK-B</sup> and AC<sup>PtNP</sup> (AC<sup>EUK-B/PtNP</sup>). b) The HepG2 cell viability after exposure to three doses of either 0.2 (ii) or 0.3 mM (iii) H<sub>2</sub>O<sub>2</sub> over 9 h depending on the different types of floating paper chips ( $n = 5$ ). The statistical significance used to compare the means was determined using a one-way analysis of variance (one-way ANOVA) followed by a Tukey's multiple comparison post hoc test ( $*p < 0.05$ ). c) i) HepG2 cells were exposed to three doses of H<sub>2</sub>O<sub>2</sub> followed by a 48 h recovery period in new media and exposure to two additional doses of H<sub>2</sub>O<sub>2</sub> (0.1–0.5 mM) before the HepG2 cell viability was assessed depending whether the AC<sup>EUK-B</sup>-loaded paper chips remained or were removed after the 48 h recovery period. ii) The dose response curve of HepG2 cells exposed to 0.1–0.5 mM H<sub>2</sub>O<sub>2</sub> when the AC<sup>EUK-B</sup>-loaded paper chips either remained floating on the wells or were removed from the cell cultures after the 48 h recovery ( $n = 4$ ). The dose response curves are fitted with a sigmoidal curve to obtain EC<sub>50</sub> values. The statistical significance used to compare the means of EC<sub>50</sub> values was determined using a one-way analysis of variance (one-way ANOVA) followed by a Tukey's multiple comparison post hoc test.  $*p < 0.05$  ( $n = 4$ ).

### 2.3. Effect of antioxidant microgels on tert-butyl hydroperoxide (tBuOOH)-challenged HepG2 cells

In addition to H<sub>2</sub>O<sub>2</sub>, tert-butyl hydroperoxide (tBuOOH) is another commonly used agent to induce oxidative stress in short-term cell cultures. tBuOOH and other organic peroxides decompose to other alkoxyl and peroxy radicals, facilitated by metal ions, resulting in the generation of ROS including H<sub>2</sub>O<sub>2</sub>. tBuOOH is commonly used in cell culture experiments due to its increased stability over H<sub>2</sub>O<sub>2</sub>, and Alía et al. found that tBuOOH gave a more consistent cellular stress response with respect to cell viability, intracellular ROS, reduced glutathione levels, mal-

ondialdehyde levels (as indicator of lipid peroxidation) and the activity of antioxidant enzymes.<sup>[41]</sup>

First, tBuOOH was successfully removed from solution when floating AC<sup>EUK-B</sup> loaded paper chips were present (Figure 3a). ≈30% tBuOOH remained after 4 h, which was comparable to the H<sub>2</sub>O<sub>2</sub> removal after 3 h (Figure 1a). Second, the HepG2 cells in the same set-up as above were stressed with 0.1–0.5 mM tBuOOH for 4 h in the presence of AC<sup>EUK-B</sup>-loaded paper chips before their viability was measured to obtain dose response curves (Figure 3b). The EC<sub>50</sub> value for paper chips loaded with AC<sup>0</sup> and empty paper chips were comparable (≈135 and 127 μM, respectively), while the presence of AC<sup>EUK-B</sup>-loaded paper chips resulted

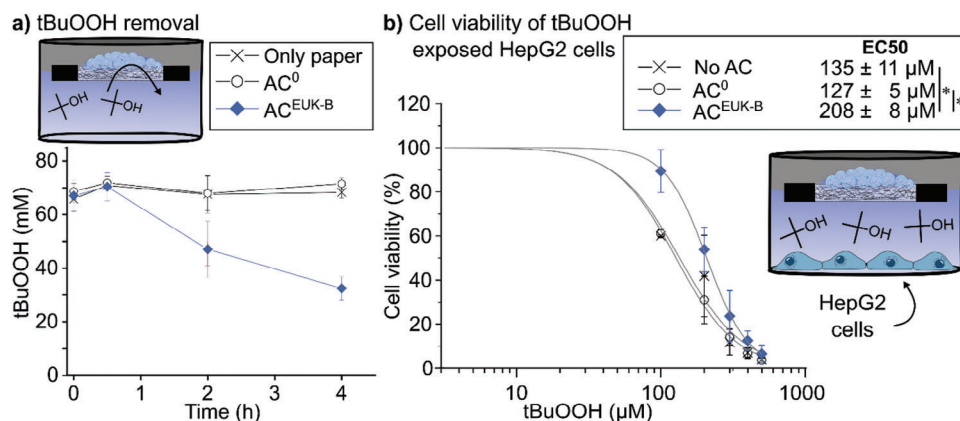


**Figure 3.** a) Conversion of tBuOOH over 4 h in the presence of empty, AC<sup>0</sup>- or AC<sup>EUK-B</sup>-loaded paper chips ( $n = 3$ ). b) Dose response curves of HepG2 cells exposed to 0.1–0.5 mM tBuOOH in wells with empty, AC<sup>0</sup>-, AC<sup>EUK-B</sup>-loaded paper chips ( $n = 3$ ). The dose response curves are fitted and the resulting EC<sub>50</sub> values are shown. The statistical significance used to compare the means of EC<sub>50</sub> values was determined using a one-way analysis of variance (one-way ANOVA) followed by a Tukey's multiple comparison post hoc test ( $*p < 0.05$ ).

in a statistically significantly higher EC<sub>50</sub> value ( $\approx 208 \mu\text{M}$ ), confirming the prior observed rescue ability of AC<sup>EUK-B</sup>.

## 2.4. Effect of Antioxidant Microgels on tBuOOH-challenged HHL-5 cells

The next aim was to evaluate the antioxidative potential of the AC<sup>EUK-B</sup> using a more physiologically relevant hepatic cell line. Specifically, the human hepatocyte line HHL-5, which is more akin to primary hepatocyte phenotype, was used as an alternative to the hepatic tumor derived HepG2 cell line.<sup>[43]</sup> The HHL-5 cells were exposed to 0.1–0.3 mM tBuOOH for 3 h in the presence of paper chips loaded with 100 mg AC<sup>EUK-B</sup> (corresponding to  $\approx 0.05$  mg EUK-B) or AC<sup>0</sup> before the cell viability and the intracellular ROS levels were assessed (Figure 4a). We would like to note that only a single dose of tBuOOH was used in this case due to its higher stability in cell culture medium and better suitability for cell experiments. As expected, the presence of AC<sup>0</sup>-loaded paper chips resulted in similar tBuOOH dose response curves in HHL-5 cells as was noted for HHL-5 cells with empty paper chips (EC<sub>50</sub>  $\approx 190 \mu\text{M}$ ) (Figure 4b). In contrast, AC<sup>EUK-B</sup>-loaded paper chips led to a statistically significantly higher EC<sub>50</sub> value ( $\approx 360 \mu\text{M}$ ) derived from dose response curves of tBuOOH exposed HHL-5 cells.

Additionally, the neutral red uptake assay was introduced as an alternative method for assessing cell viability, in place of the previously used CCK-8 assay. The neutral red uptake assay relies on the accumulation of a cationic dye called neutral red within the lysosomes of cells. The retention of this dye is directly influenced by the lysosomal buffering capacity of the cells, and subsequently, it correlates with the number of viable cells, similar to the formazan dye produced by cellular dehydrogenases in the CCK-8 assay. The HHL-5 cells were incubated with neutral red followed by the extraction of the dye from viable cells with an acidic EtOH solution before the absorbance ( $\lambda_{\text{abs}} = 540 \text{ nm}$ ) of the media was measured to determine dose response curves (Figure 4ci). The presence of AC<sup>EUK-B</sup>-loaded paper chips led to qualitatively more neutral red being sequestered in the lysosomes, suggest-

ing that the cells maintained their pH gradients due to a maintained ATP production.<sup>[44]</sup> Although a similar trend to that observed with the CCK-8 assays was found, the EC<sub>50</sub> values obtained for HHL-5 cells in the presence of AC<sup>EUK-B</sup>-loaded paper chips ( $\approx 370 \mu\text{M}$ ) did not exhibit significant differences when compared to the non-treated HHL-5 cells or HHL-5 cells in the presence of AC<sup>0</sup>-loaded paper chips ( $\approx 200 \mu\text{M}$ ), primarily due to the higher error associated with this particular method. Additionally, HHL-5 cells, when treated with 0.2 mM tBuOOH as an exemplary concentration, displayed a diminished neutral red signal within the lysosomes and a reduction in the number of cells compared to the untreated HHL-5 cells, when imaged with bright field microscopy (Figure 4cii). However, the tBuOOH-stressed HHL-5 cells treated with AC<sup>EUK-B</sup> showed an increase in the lysosomal sequestering of neutral-red compared to the non-treated tBuOOH-stressed HHL-5 cells. Considering the results collectively, AC<sup>EUK-B</sup> demonstrated a positive impact on the viability of tBuOOH-stressed HHL-5 cells, indicating its potential beneficial effect under these conditions.

Finally, we aimed to evaluate whether improved HHL-5 cell viability could be correlated with a decrease in intracellular ROS. To this end, 6-carboxy-2',7'-dichlorodihydrofluorescein diacetate (carboxy-H<sub>2</sub>DCFDA), which is internalized and converted to the deacetylated, oxidized, and fluorescent product carboxydichlorofluorescein (carboxy-DCF) in the presence of ROS, was used as an indicator for intracellular ROS. HHL-5 cells were challenged with 0.2 mM tBuOOH for 3 h in the presence of empty, or AC<sup>0</sup>-, or AC<sup>EUK-B</sup>-loaded paper chips, and then imaged using fluorescence microscopy. As anticipated, HHL-5 cells exposed to tBuOOH in the presence of empty or AC<sup>0</sup>-loaded paper chips had an increase in carboxy-DCF signal originating from the higher ROS levels compared to pristine HHL-5 cells. Importantly, HHL-5 cells in the presence of AC<sup>EUK-B</sup>-loaded paper chips, had a clear decrease in carboxy-DCF signal, suggesting lower ROS levels (Figure 4di). Further, the mean fluorescence intensity of the signal originating from carboxy-DCF was quantitated by determining the average of all pixel intensities in a region of interest,<sup>[45]</sup> before the background corrected pixel intensities of each sample were normalized to HHL-5 cells exposed to 0.2 mM

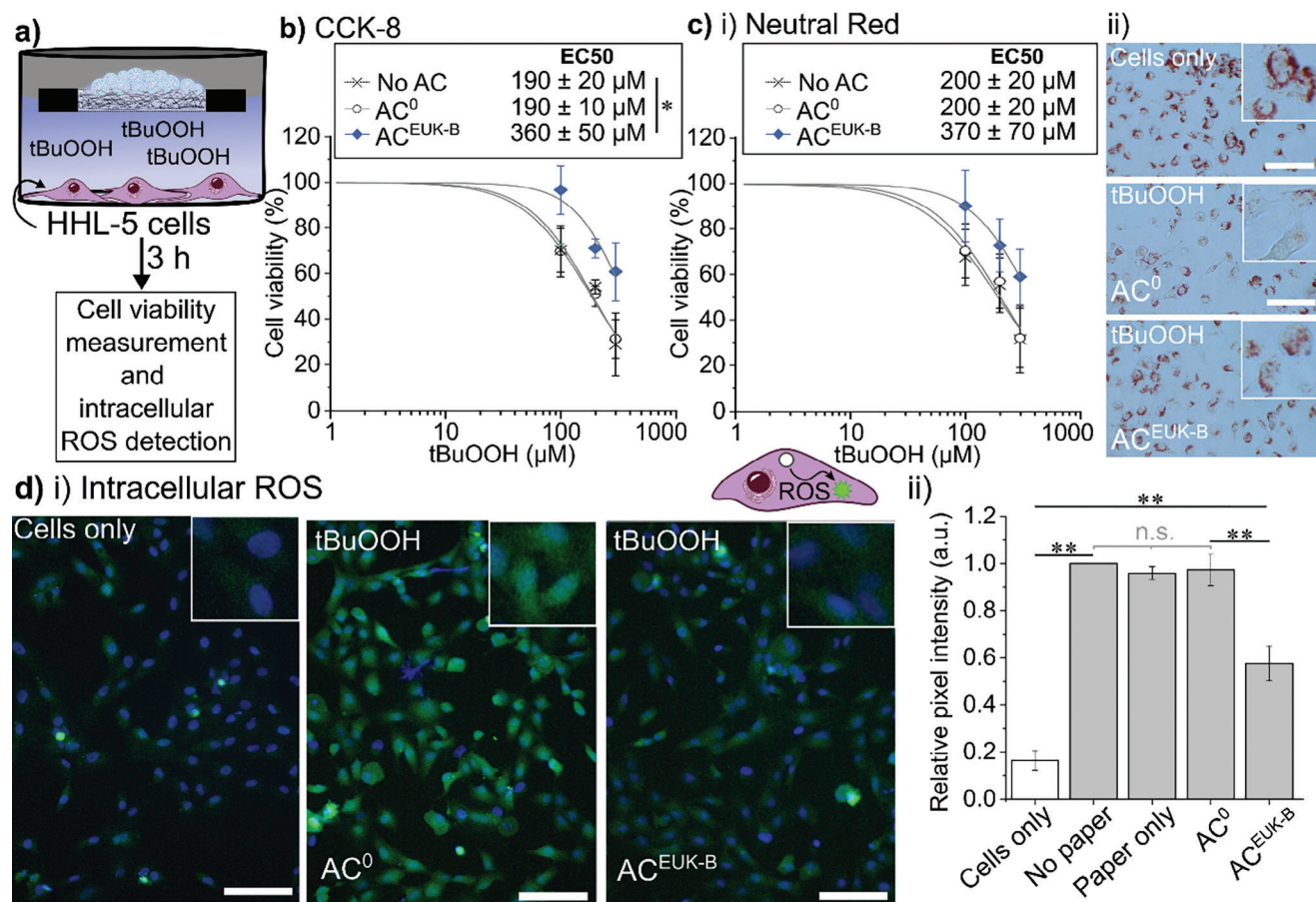


**Figure 4.** a) HHL-5 cells were exposed to tBuOOH for 3 h before the cell viability and the intracellular ROS levels were determined. Viability measured with CCK-8 (b) or the neutral red uptake assay (c) of HHL-5 cells upon exposure to 0.1–0.3 mM tBuOOH in the presence of empty, or AC<sup>0</sup>, or AC<sup>EUK-B</sup>-loaded paper chips ( $n = 3$ ). ci) HHL-5 cell viability evaluated based on the absorbance of the media following de-staining. ii) Representative bright field images of 0.2 mm tBuOOH-challenged HHL-5 cells incubated with neutral red. Scale bars = 100 μm. d) i) Representative fluorescence microscopy images of 0.2 mm tBuOOH-challenged HHL-5 cells in the presence of empty, AC<sup>0</sup>, or AC<sup>EUK-B</sup>-loaded paper chips incubated with 6-carboxy-2',7'-dichlorodihydrofluorescein diacetate (carboxy-H<sub>2</sub>DCFDA), which is converted to the fluorescent carboxy-dichlorofluorescein (carboxy-DCF) in the presence of intracellular ROS ( $n = 3$ ). Scale bars = 100 μm. ii) The pixel intensity in the images originating from the fluorescent carboxy-DCF was quantified using ImageJ. A minimum of five images of each condition was used per repeat ( $n = 3$ ). The statistical significance used to compare the means was determined using a one-way analysis of variance (one-way ANOVA) followed by a Tukey's multiple comparison post hoc test. \* $p < 0.05$ , \*\* $p < 0.005$ , n.s. = not significant.

tBuOOH in absence any of paper chips (Figure 4dii). A significantly lower relative pixel intensity was observed for tBuOOH-challenged HHL-5 cells in the presence of AC<sup>EUK-B</sup>-loaded paper chips (≈40%) compared to HHL-5 cells in all other cases, supporting the positive impact of AC<sup>EUK-B</sup> on cell viability.

### 3. Conclusion

We report the fabrication of antioxidant artificial cells loaded with artificial enzymes, AC<sup>PtNP</sup> and AC<sup>EUK-B</sup>, with catalase- and SOD-like activity. The AC<sup>EUK-B</sup> was found to exhibit higher catalytic activity than AC<sup>PtNP</sup>, and the beneficial effect of the antioxidant microgel AC<sup>EUK-B</sup> on the viability and intracellular ROS of peroxide challenged hepatic cells was demonstrated. Oxidative stress is implicated in a wide range of pathologies, and thus AC<sup>EUK-B</sup> could be explored in numerous contexts. Future work could focus on developing more relevant oxidative stress cell models, which bet-

ter mimic the long-term ROS exposure in disease, allowing for elucidating the supportive effect of AC<sup>EUK-B</sup> in details. Eventually, these findings could potentially pave the way for more translational approaches in AC design to lower ROS in liver disease. The use of stable and long-lived artificial enzymes encapsulated in hydrogel microgels, which can be fabricated in bulk, can be implemented as a supplementary approach, e.g., in extracorporeal liver support devices.

### 4. Experimental Section

**Materials:** 4-(2-hydroxyethyl)piperazine-1-ethane-sulfonic acid (HEPES, >99.5%), sodium chloride (NaCl), hydrochloric acid (HCl), sodium hydroxide (NaOH), dimethyl sulfoxide (DMSO), phosphate buffered saline (PBS), 0.25% trypsin-EDTA, calcium chloride dihydrate (CaCl<sub>2</sub>, purity ≥99.0%), cell counting kit CCK-8, hydrogen peroxide (H<sub>2</sub>O<sub>2</sub>, 30% (w/w)), o-dianisidine, SOD determination kit (19160), hexachloroplatinic acid, sodium borohydride, trisodium citrate, o-

dianisidine, SOD determination kit (19160), minimum essential medium eagle (MEME, M2279, Sigma Aldrich), MEM non-essential amino acid solution, ethanol 96%, and Neutral Red were purchased from Sigma Aldrich. Fetal bovine serum (FBS), DMEM glucose free (11966025), sodium pyruvate, L-glutamine, GlutaMAX, streptomycin, and penicillin, qualitative filter papers grade 600 (516-0309), dichlorodihydrofluorescein diacetate (carboxy-H<sub>2</sub>DCFDA), and tert-butyl hydroperoxide (70% solution in water) were purchased from Thermo Fisher Scientific. Ultrapure low molecular weight sodium alginate with high  $\alpha$ -L-guluronate (G block) ( $M_w < 75$  kDa,  $\geq 60\%$  G block content, PRONOVA, UP VLVG), ultrapure high molecular weight sodium alginate with high G block content ( $M_w > 200$  kDa,  $\geq 60\%$  G block content, PRONOVA, UP MVG) was purchased from NovaMatrix.

HEPES buffer consisted of 10 mM HEPES and 150 mM NaCl at pH 7.4. Ultrapure water (18.2 M $\Omega$  cm resistance) was provided by an ELGA Purelab Ultra system (ELGA LabWater, Lane End).

**Platinum Nanoparticles (PtNPs):** PtNPs were synthesized based on a previously published protocol.<sup>[4]</sup> Briefly, 1 mL of a hexachloroplatinic acid solution (H<sub>2</sub>PtCl<sub>6</sub>) (32 mM in ultrapure water) was mixed with 1 mL of a trisodium citrate solution (80 mM in ultrapure water) and 32 mL ultrapure water and left to stir for 30 min at room temperature. Then, 400  $\mu$ L of a NaBH<sub>4</sub> solution (100 mM) was added, which turned the solution dark brown, and was left under stirring for 1 h at room temperature, to yield citrate-capped PtNPs. PtNPs were visualized using transmission electron microscopy (TEM). And 300 mesh copper formvar/carbon grids were treated with glow discharging, and 4  $\mu$ L of PtNP solution were added to the grid. The solution was left to adsorb for 30 s before blotting the excess sample. TEM images were taken with a Tecnai G2 Spirit Instrument (TWIN/BioTWIN, FEI co.). The size distribution was measured from 150 PtNPs from a single repeat. Additionally, 5 mL of the PtNP solution was heated to 80 °C for 3 days to completely evaporate the ultrapure water, and the remaining powder was weighed to evaluate the mass of PtNPs to be encapsulated in the microgels.

**Microgel Preparation:** PtNPs and EUK-B were directly encapsulated in alginate-based microgels to yield AC<sup>PtNP</sup> or AC<sup>EUK-B</sup>. Specifically, 37.5 mg UP MVG alginate was mixed with 37.5 mg UP VLVG alginate (Pronova) and dissolved overnight in either 5 mL of the PtNP stock solution (final alginate concentration of 15 mg mL<sup>-1</sup>). Alternatively, 37.5 mg UP MVG alginate was mixed with 37.5 mg UP VLVG alginate and dissolved in 43.10  $\mu$ L HEPES buffer overnight. Then, the 17.4 mg mL<sup>-1</sup> alginate solution was added dropwise over  $\approx 10$  min to 690  $\mu$ L of a 33.3 mg mL<sup>-1</sup> EUK-B in DMSO solution while vortexing to yield a final concentration of EUK-B of 0.46 mg mL<sup>-1</sup> and 15 mg mL<sup>-1</sup> alginate. Empty microgels, AC<sup>0</sup>, were made by mixing 37.5 mg UP MVG alginate with 37.5 mg UP VLVG alginate followed by dissolving in 5 mL HEPES buffer. The resulting alginate solutions were loaded into a 20 mL syringe and connected to an Encapsulator B-390 (Buchi). A 200  $\mu$ m inner and a 300  $\mu$ m outer nozzle were used to form microgels of  $\approx 200$   $\mu$ m. The syringe was fixed onto a pump and injected at a speed of 1.1 mL min<sup>-1</sup>. A frequency of 1300 Hz, a pressure of 0.945 mbar, a voltage of 800 V, and an air flow of 0.5 NI min<sup>-1</sup> was used during microgel fabrication. The cross-linked particles were collected in a glass beaker containing 0.1 M CaCl<sub>2</sub> under stirring, and were collected in a 40  $\mu$ m cell strainer (Corning). The initial encapsulation efficiency was evaluated by taking photographs of Eppendorf tubes containing the microgels in some of the CaCl<sub>2</sub> collection bath, while the leakage was visually assessed by imaging microgels stored in PBS with 0.01 M CaCl<sub>2</sub> after 5 days or 12 months. The alginate microgels were visualized using an inverted Olympus microscope (IX81), and the size distribution was assessed from the images using ImageJ. The size distribution was fitted with a Gaussian Amplitude function with Origin software, and the sizes are given as  $\mu \pm 2\sigma$ . A minimum of 300 particles were measured for each sample from three independent repeats.

**Preparation of Paper Chip:** The paper chips were prepared using a previously published protocol.<sup>[42]</sup> The diameter of the circular paper chips was chosen to have an inner and outer diameter of 1.3 and 2.0 cm to fit into a 12-well plate, and the width of the printed ring 0.35 cm. A central cross with a width of 0.1 cm was included to improve the floating of the paper chips. The pattern on the circular paper chips was designed in Mi-

crosoft Powerpoint and printed onto both sides of an A0 VWR qualitative filter paper grade 600 (516 0309), which was cut to an A4 size, using a Laserjet printer (Xerox WorkCentre 7845). The printed sheets were autoclaved to melt the ink particles that resulted in a hydrophobic barrier that allows the paper chip to float on aqueous solutions. The individual circular paper chips were cut out under sterile conditions when used in cell experiments, and applied to the top of the wells using a tweezer.

**Hydrogen Peroxide (H<sub>2</sub>O<sub>2</sub>) and tert-Butyl Hydroperoxide (tBuOOH) Detection Assay:** H<sub>2</sub>O<sub>2</sub> and tBuOOH concentrations were detected to determine the PtNP and EUK-B activity. First, the activity of the free PtNP and EUK-B were compared by dissolving 0.1 mg of either PtNPs or EUK-B in 1.5 mL of 1 mM H<sub>2</sub>O<sub>2</sub> in PBS, in a 12 well plate. After 1, 2, 4, 6, 8, and 10 min, the amount of remaining H<sub>2</sub>O<sub>2</sub> was quantified by transferring 2.5  $\mu$ L of the solutions to a 96 well plate, followed by the addition of 7.5  $\mu$ L PBS and 50  $\mu$ L reaction mixture consisting of 0.13 mM *o*-dianisidine hydrochloride and 2 U mL<sup>-1</sup> Horse Radish Peroxidase in ultrapure water. The absorbance was monitored ( $\lambda = 440$  nm) using a multiplate reader (Perkin Elmer) immediately after adding the reaction mixture. The absorbance of solutions without H<sub>2</sub>O<sub>2</sub> was measured as backgrounds to take into account the color of the EUK-B and PtNP compounds. A standard curve (25–1000  $\mu$ M H<sub>2</sub>O<sub>2</sub>) was prepared in PBS buffer and linear regression was used to determine H<sub>2</sub>O<sub>2</sub> concentrations. Alternatively, 100 mg of AC<sup>PtNP</sup>, AC<sup>EUK-B</sup>, or AC<sup>0</sup> was weighed off and placed on top of a floating paper chip in a 12 well plate containing 1350  $\mu$ L of either ultrapure water, PBS or cell media. 150  $\mu$ L of 10 mM H<sub>2</sub>O<sub>2</sub> was added to each well (final concentration of 1 mM H<sub>2</sub>O<sub>2</sub>). Wells with 1 mM H<sub>2</sub>O<sub>2</sub> in ultrapure water, PBS or cell media without any paper chip or only a paper chip without any microgels were prepared as controls for the natural decomposition of H<sub>2</sub>O<sub>2</sub>. 10  $\mu$ L from each well was taken out after 1, 3, 6, or 8 h and the H<sub>2</sub>O<sub>2</sub> concentration was detected immediately by adding 50  $\mu$ L reaction mixture as described above. A standard curve (25–1000  $\mu$ M H<sub>2</sub>O<sub>2</sub>) was prepared in ultrapure water, PBS buffer or cell media and linear regression was used to determine H<sub>2</sub>O<sub>2</sub> concentrations. Alternatively, the assay was performed with tBuOOH, where the removal of 70 mM tBuOOH was followed over 4 h in PBS. It should be noted that the *o*-dianisidine-based assay could only detect the conversion when significantly higher concentrations of tBuOOH were used compared to H<sub>2</sub>O<sub>2</sub>. Three independent repeats in triplicate were performed for each experiment.

**Superoxide Dismutase (SOD) Activity Assay:** SOD activity was evaluated using a commercially available kit (19160, Sigma Aldrich) and the WST working solution and enzyme working solution was prepared according to the manufacturer's protocol. 1, 2.5, 5, or 10 mg AC<sup>PtNP</sup>, AC<sup>EUK-B</sup> or AC<sup>0</sup> were added to floating paper chips in a 12 well plate. Each well contained 100  $\mu$ L ultrapure water, 1000  $\mu$ L WST working solution and 100  $\mu$ L enzyme working solution. Negative controls were included where no enzyme working solution (blank) or no microgels were added. The plate was left for 30 min at 37 °C before 100  $\mu$ L was transferred from each well to a 96 well plate, and the absorbance was monitored ( $\lambda = 450$  nm) using a multiplate reader (Perkin Elmer). The SOD-like activity is given as

$$\text{Inhibition rate (\%)} = \frac{(\text{Abs}_{\text{no microgel}} - \text{Abs}_{\text{blank}}) - (\text{Abs}_{\text{sample}} - \text{Abs}_{\text{blank}})}{\text{Abs}_{\text{no microgel}} - \text{Abs}_{\text{blank}}} \times 100.$$

Three independent repeats in triplicate were performed for each experiment.

**Culturing of HepG2 Cells:** The human liver cancer cell line HepG2 was purchased from European Collection of Cell Cultures. HepG2 cells were cultured in 75 cm<sup>2</sup> (TC-treated) culture flasks in glucose free DMEM at 37 °C and 5% CO<sub>2</sub>. The media was supplemented with 10% FBS, 2 mM glutamine, 100  $\mu$ g mL<sup>-1</sup> streptomycin, and 100 U mL<sup>-1</sup> penicillin, 10 mM galactose, and 1 mM sodium pyruvate.

**Cell Viability of H<sub>2</sub>O<sub>2</sub>- or tBuOOH-Challenged HepG2 Cells:** 1 mL of 500  $\times 10^3$  HepG2 cells mL<sup>-1</sup> were seeded per well in a 12 well plate, and left to adhere overnight at 37 °C and 5% CO<sub>2</sub>. Then, the cell media was exchanged to 1350  $\mu$ L media and the floating paper chips were added to each well. 100 mg of AC<sup>0</sup>, AC<sup>PtNP</sup>, or AC<sup>EUK-B</sup> were added to each paper chip. Alternatively, 50 mg AC<sup>PtNP</sup> and 50 mg AC<sup>EUK-B</sup> were added to each paper chip, referred to as AC<sup>EUK-B/PtNP</sup>. Three doses of 150  $\mu$ L of 1–5 mM H<sub>2</sub>O<sub>2</sub> were added to each well over 9 h with 3 h intervals (final concentrations of 0.1–0.5 mM H<sub>2</sub>O<sub>2</sub>). During the 9 h H<sub>2</sub>O<sub>2</sub> exposure, the cells were



left to incubate while shaking at 37 °C and 5% CO<sub>2</sub>. Then, the cell viability was measured using CCK-8 solution after removing the paper chips. The HepG2 cells were washed once with PBS, and 1000 µL of cell medium containing 25 µL of CCK-8 was added to each well of a 12 well plate. The plates were left to incubate for 2 h at 37 °C in 5% CO<sub>2</sub> before 100 µL media were transferred to each well of a 96-well plate, and the absorbance ( $\lambda = 450$  nm) was monitored using a multimode plate reader (Perkin Elmer). If required, the HepG2 cells were left to recover for 48 h after the 9 h H<sub>2</sub>O<sub>2</sub> exposure before the paper chips were either left or removed from the wells and two additional doses of 150 µL of 1–5 mM H<sub>2</sub>O<sub>2</sub> were added to each well 3 h apart followed by the cell viability assessment using CCK-8. Four independent repeats in triplicate were performed for each experiment. Alternatively, the HepG2 cells were exposed to 0.1–0.5 mM tBuOOH for 4 h in the presence of microgel-loaded paper chips before the CCK-8 assay was performed as outlined above. Three independent repeats in triplicate were performed for each experiment.

**Culturing of HHL-5 Cells:** The work on the immortalized human liver cell line HHL-5 was conducted at ILDH, UCL, London. HHL-5 cells were cultured in 75 cm<sup>2</sup> (TC-treated) culture flasks in either MEME or glucose free DMEM at 37 °C and 5% CO<sub>2</sub>. All media were supplemented with 10% FBS, 2 mM GlutaMAX, 100 µg mL<sup>-1</sup> streptomycin, and 100 U mL<sup>-1</sup> penicillin. In addition, 1% MEM nonessential amino acid solution was added to the MEME media, and 10 mM galactose and 1 mM sodium pyruvate was added to the glucose free cell media.

**Cell Viability of tBuOOH-Challenged HHL-5 Cells:** 1 mL of 150 × 10<sup>3</sup> HHL-5 cells mL<sup>-1</sup> were seeded per well in a 12 well plate and left to adhere overnight at 37 °C and 5% CO<sub>2</sub>. Then, the cell media was exchanged to 1350 µL media, and 150 µL of 2–5 mM tBuOOH was added to each well (final concentrations of 200–500 µM tBuOOH), and the floating paper chips were added to each well. 100 mg of AC<sup>0</sup> or AC<sup>EUK-B</sup> were added to each paper chip. The HHL-5 cells were left to incubate while shaking at 37 °C and 5% CO<sub>2</sub> for 3 h. The HHL-5 cell viability was assessed using CCK-8 (as described above for HepG2 cells) or the neutral red uptake assay. In the latter case, neutral red was dissolved in PBS (4 mg mL<sup>-1</sup>), followed by dilution 100× in FBS-free media to give a saturated neutral red (40 µg mL<sup>-1</sup>) solution, which was then left at 37 °C in 5% CO<sub>2</sub> overnight. Then, the neutral red solution was centrifuged at 600g for 10 min to sediment the precipitates. The HHL-5 cells were washed once with PBS before 1 mL of neutral red containing cell medium was added to each well and let to incubate for 3 h at 37 °C in 5% CO<sub>2</sub> followed by washing extensively (≈5–10× with PBS) until no neutral red precipitate was observed in the microscope. Each well was imaged in 300 µL HBSS using bright field microscopy. Then, the HBSS was removed from each well and 500 µL de-staining solution (50 v/v% ethanol (96%), 49 v/v% deionized water, 1 v/v% glacial acetic acid) was added to each well and left to incubate while shaking for 10 min at room temperature. 100 µL from each well was transferred to a 96 well plate, and the absorbance ( $\lambda = 540$  nm) was measured using a multimode plate reader. Three independent repeats in triplicate were performed for each experiment.

**Intracellular ROS in HHL-5 Cells:** The HHL-5 cells were challenged with tBuOOH as outlined above using microgel-loaded paper chips before washing 2× with PBS and followed by the addition of 500 µL carboxy-H<sub>2</sub>DCFDA solution (25 µM in PBS) to each well. The cells were left to incubate for 30 min at 37 °C in 5% CO<sub>2</sub>. In the last 5 min, Hoechst 33342 was added at 1 v/v% for a final concentration of 1 µM. The HHL-5 cells were washed 2× in PBS, and 300 µL PBS was added to each well followed by imaging using epifluorescence microscopy. The settings during imaging were kept constant allowing for quantification of the pixel intensities in the carboxy-DCF channel. The images were analyzed using ImageJ. A threshold (5–255) was applied to each image to exclude background pixels and select the region of interest (the intracellular space). The mean pixel intensities from the cells were measured from min. 5 images. The mean pixel intensities were normalized to the mean pixel intensity from tBuOOH-treated HHL-5 cells in the presence of empty paper chips. The relative pixel intensity from three independent repeats were measured, and a one-way analysis of variance (one-way ANOVA) followed by a Tukey's multiple comparison post hoc test was used to compare the means. Three independent repeats in duplicate were performed for each experiment.

## Supporting Information

Supporting Information is available from the Wiley Online Library or from the author.

## Acknowledgements

This project has received funding from the European Research Council (ERC) under the European Union's Horizon 2020 research and innovation program (grant agreement no. 818890). The UFM EliteForsk travel grant is acknowledged for support (Isabella Nymann Westensee).

## Conflict of Interest

A patent has been filed around this technology (ref. TECH-2023-631-481).

## Data Availability Statement

The raw data for this manuscript can be downloaded from <https://doi.org/10.5281/zenodo.10477607>.

## Keywords

antioxidants, EUK compounds, hepatocytes, hydrogels, reactive oxygen species

Received: October 10, 2023

Revised: January 9, 2024

Published online:

- [1] S. Li, H. Li, X. Xu, P. E. Saw, L. Zhang, *Theranostics* **2020**, *10*, 1262.
- [2] M. Liu, Q. Huang, Y. Zhu, L. Chen, Y. Li, Z. Gong, K. Ai, *Mater Today Bio.* **2022**, *13*, 100215.
- [3] C. O. M. Jasirwan, A. Muradi, R. D. Antarianto, *Livers* **2023**, *3*, 65.
- [4] B. C. Buddingh', J. C. M van Hest, *Acc. Chem. Res.* **2017**, *50*, 769.
- [5] S. Ausländer, D. Ausländer, M. Fussenegger, *Angew. Chem., Int. Ed.* **2017**, *56*, 6396.
- [6] W. Jiang, Z. Wu, Z. Gao, M. Wan, M. Zhou, C. Mao, J. Shen, *ACS Nano* **2022**, *16*, 15705.
- [7] C. Guindani, L. C. da Silva, S. Cao, T. Ivanov, K. Landfester, *Angew. Chem., Int. Ed.* **2022**, *61*, e202110855.
- [8] X. Qian, I. Nymann Westensee, E. Brodzki, B. Städler, *Wiley Interdiscip. Rev. Nanomed. Nanobiotechnol.* **2021**, *13*, e1683.
- [9] Y. Elani, *Angew. Chem., Int. Ed.* **2021**, *60*, 5602.
- [10] I. N. Westensee, B. Städler, *Interface Focus* **2023**, *13*, 20230007.
- [11] X. Wang, L. Tian, Y. Ren, Z. Zhao, H. Du, Z. Zhang, B. W. Drinkwater, S. Mann, X. Han, *Small* **2020**, *16*, 1906394.
- [12] Ö. D. Toparlak, J. Zasso, S. Bridi, M. D. Serra, P. Macchi, L. Conti, M.-L. Baudet, S. S. Mansy, *Sci. Adv.* **2020**, *6*, eabb4920.
- [13] F. Itef, J. Skovhus Thomsen, B. Städler, *ACS Appl. Mater. Interfaces* **2018**, *10*, 30180.
- [14] A. Armada-Moreira, E. Taipaleenmäki, M. Baekgaard-Laursen, P. S. Schattling, A. M. Sebastião, S. H. Vaz, B. Städler, *ACS Appl. Mater. Interfaces* **2018**, *10*, 7581.
- [15] A. Armada-Moreira, J. E. Coelho, L. V. Lopes, A. M. Sebastião, B. Städler, S. H. Vaz, *Adv. Biosyst.* **2020**, *4*, 2000139.
- [16] P. Chen, X. Ning, W. Li, Y. Pan, L. Wang, H. Li, X. Fan, J. Zhang, T. Luo, Y. Wu, C. Ou, M. Chen, *Bioact. Mater.* **2022**, *14*, 416.

- [17] X. Zhang, C. Li, F. Liu, W. Mu, Y. Ren, B. Yang, X. Han, *Nat. Commun.* **2022**, *13*, 2148.
- [18] J. Liu, J. Xue, L. Fu, J. Xu, M. S. Lord, K. Liang, *Adv. Funct. Mater.* **2022**, *32*, 2111271.
- [19] S. Liu, Y. Zhang, M. Li, L. Xiong, Z. Zhang, X. Yang, X. He, K. Wang, J. Liu, S. Mann, *Nat. Chem.* **2020**, *12*, 1165.
- [20] G. Chen, R. Levin, S. Landau, M. Kaduri, O. Adir, I. Ianovici, N. Krinsky, O. Doppelt-Flikshtain, J. Shklover, J. Shainsky-Roitman, S. Levenberg, A. Schroeder, *Proc. Natl. Acad. Sci. USA* **2022**, *119*, e2207525119.
- [21] X. Qian, I. N. Westensee, C. C. Fernandes, B. Städler, *Angew. Chem., Int. Ed.* **2021**, *60*, 18704.
- [22] Y. Zhang, P. S. Schattling, F. Itel, B. Städler, *ACS Omega* **2017**, *2*, 7085.
- [23] Y. Zhang, M. Baekgaard-Laursen, B. Städler, *Adv. Healthcare Mater.* **2017**, *6*.
- [24] Y. Liu, H. Wu, M. Li, J.-J. Yin, Z. Nie, *Nanoscale* **2014**, *6*, 11904.
- [25] A. Clark, A. Zhu, K. Sun, H. R. Petty, *J. Nanopart. Res.* **2011**, *13*, 5547.
- [26] M. Moglianetti, E. De Luca, D. Pedone, R. Marotta, T. Catelani, B. Sartori, H. Amenitsch, S. F. Retta, P. P. Pompa, *Nanoscale* **2016**, *8*, 3739.
- [27] S. Gunes, Z. He, D. van Acken, R. Malone, P. J. Cullen, J. F. Curtin, *Nanomedicine: NBM* **2021**, *36*, 102436.
- [28] D.-Y. Zhang, H. Liu, M. R. Younis, S. Lei, C. Yang, J. Lin, J. Qu, P. Huang, *Chem. Eng. J.* **2021**, *409*, 127371.
- [29] P. Pfeiffer, E. Breith, E. Lübbe, T. T. N Tsumaki, *Justus Liebig's Ann. Chem.* **1933**, *503*, 84.
- [30] L. Rouco, A. M. González-Noya, R. Pedrido, M. Maneiro, *Antioxidants* **2020**, *9*, 727.
- [31] L. Declercq, I. Sente, L. Hellemans, H. Corstjens, D. Maes, *Int. J. Cosmet. Sci.* **2004**, *26*, 255.
- [32] A. Kumar, S. Shukla, A. K. Chauhan, D. Singh, H. P. Pandey, C. Singh, *Chem. Biol. Interact.* **2015**, *231*, 18.
- [33] S. Magder, D. G. Parthenis, I. A. Ghoulah, *Int. J. Mol. Sci.* **2015**, *16*, 6801.
- [34] R. A. Rosenthal, B. Fish, R. P. Hill, K. D. Huffman, Z. Lazarova, J. Mahmood, M. Medhora, R. Molthen, J. E. Moulder, S. T. Sonis, P. J. Tofilon, S. R. Doctrow, *Anticancer Agents Med. Chem.* **2011**, *11*, 359.
- [35] M. D. Howard, C. F. Greineder, E. D. Hood, V. R. Muzykantov, *J. Control Release* **2014**, *177*, 34.
- [36] J. Dessolin, M. Schuler, A. Quinart, F. De Giorgi, L. Ghosez, F. Ichas, *Eur. J. Pharmacol.* **2002**, *447*, 155.
- [37] A. Rezazadeh, R. Yazdanparast, M. Molaei, *J. Biomed. Sci.* **2012**, *19*, 26.
- [38] C. Ade, E. Brodzkij, B. Thingholm, N. Gal, F. Itel, E. Taipaleenmäki, M. J. Hviid, P. S. Schattling, B. Städele, *ACS Appl. Polym. Mater.* **2019**, *1*, 1532.
- [39] K. Y. Lee, D. J. Mooney, *Prog. Polym. Sci.* **2012**, *37*, 106.
- [40] H. Sies, *Redox Biol.* **2017**, *11*, 613.
- [41] M. Alía, S. Ramos, R. Mateos, L. Bravo, L. Goya, *J. Biochem. Mol. Toxicol.* **2005**, *19*, 119.
- [42] P. De Dios Andres, I. N. Westensee, E. Brodzkij, M. A. Ramos-Docampo, N. Gal, B. Städler, *Biomacromolecules* **2021**, *22*, 3860.
- [43] R. F. Clayton, A. Rinaldi, E. E. Kandyba, M. Edward, C. Willberg, P. Klenerman, A. H. Patel, *Liver Int.* **2005**, *25*, 389.
- [44] G. Repetto, A. Peso, J. L Zurita, *Nat. Protoc.* **2008**, *3*, 1125.
- [45] M. H. Shihan, S. G. Novo, S. J. Le Marchand, Y. Wang, M. K. Duncan, *Biochem. Biophys. Rep.* **2021**, *25*, 100916.